Available online at www.sciencedirect.com
ScienceDirect
Journal of Sound and Vibration 319 (2009) 445–462
JOURNAL OF SOUND AND VIBRATION
www.elsevier.com/locate/jsvi

Exploring the performance of a nonlinear tuned mass damper

Nicholas A. Alexander[a,*], Frank Schilder[b]

[a]Department of Civil Engineering, University of Bristol, Bristol BS81 TR, UK
[b]Department of Mathematics, University of Surrey, Guildford GU2 7XH, UK

Received 15 February 2008; received in revised form 7 May 2008; accepted 12 May 2008
Handling Editor: M.P. Cartmell
Available online 24 June 2008

Abstract

We explore the performance of a nonlinear tuned mass damper (NTMD), which is modeled as a two degree of freedom system with a cubic nonlinearity. This nonlinearity is physically derived from a geometric configuration of two pairs of springs. The springs in one pair rotate as they extend, which results in a hardening spring stiffness. The other pair provides a linear stiffness term. We perform an extensive numerical study of periodic responses of the NTMD using the numerical continuation software AUTO. In our search for optimal design parameters we mainly employ two techniques, the optimization of periodic solutions and parameter sweeps. During our investigation we discovered a family of *detached resonance curves* for vanishing linear spring stiffness, a feature that was missed in an earlier study. These detached resonance response curves seem to be a weakness of the NTMD when used as a passive device, because they essentially restore a main resonance peak. However, since this family is *detached* from the low-amplitude responses there is an opportunity for designing a semi-active device.

1. Introduction

The philosophy employed in the design of most building structures in seismic zones involves inelastic and nonlinear building behavior [1,2]. This design approach mitigates the seismic hazard by allowing the structure to become damaged. Thus introducing the well-known strength reduction factors [3]. Ideally, in the case of frame structures, the damage is mostly restricted to the horizontal elements (e.g. beams) rather than the vertical elements (e.g. columns). Thus, it avoids various local failure mechanisms, such as soft-story failures, that are highly undesirable. This approach is thought to be cost effective at the design and build stage of a structure. However, in the case of a significant seismic event the damage caused often imposes considerable additional cost. It is not unusual to be forced to demolish and completely reconstruct a building after a large earthquake. Hence, this design philosophy can suffer from significant financial penalties in the event of a large earthquake. For example the Northridge event (USA, 1994) produced an estimated $12.5 billion in damages [4].

*Corresponding author.
E-mail address: nick.alexander@bristol.ac.uk (N.A. Alexander).

0022-460X/$ - see front matter © 2008 Elsevier Ltd. All rights reserved.
doi:10.1016/j.jsv.2008.05.018

Nomenclature

A	forcing amplitude
A_e	forcing amplitude value at which the total intensity of the forcing is equal to the Kanai–Tajimi seismic event
c	damping coefficient of building
c_2	damping coefficient of NTMD
D	seismic event duration (t)
$F(\omega)$	frequency dependent forcing amplitude
G_0	Kanai–Tajimi amplitude parameter
h	building height
$H_s(\omega)$	support/building transfer function
$H_{\mathrm{kt}}(\omega)$	Kanai–Tajimi spectrum
k_b	building flexural stiffness function when subject to lateral movement
k_l	stiffness of one of the linear spring components of NTMD
k_g	stiffness of one linear spring used as part of geometric nonlinear component of NTMD
k_N	stiffness of nonlinear spring component of NTMD
k_2	stiffness of both linear spring components of NTMD
m	building mass per unit height
m_2	mass of mass damper attachment
t	time
$x_0(t)$	ground displacement
$x_1(t)$	displacement of top of building (absolute ordinate)
$x_2(t)$	displacement of NTMD (absolute ordinate)
$y(z,t)$	building displacement
$y_1(t)$	building displacement (relative to foundations) at top of building
$y_2(t)$	displacement (relative to foundations) of NTMD
α	equation adjustment parameter, $\alpha = 1$ in this paper, $\alpha = 0$ in Ref. [15]
ε	mass ratio of NTMD to building.
γ_1	ratio of critical damping of building
γ_2	ratio of critical damping of NTMD
γ_g	Kanai–Tajimi averaged damping ratio of near surface geology
$\phi(z)$	building displacement shape function (normalized)
ρ	participation parameter, this can be obtained from a modal analysis of the building structure using finite element method. In this paper $\rho = -4/10$ is used
τ	scaled time
ω	ratio of forcing frequency to building natural frequency
ω_1	natural circular frequency of building
ω_2	frequency parameter (linear component of NTMD)
Ω	ratio of frequency parameter (linear component of NTMD) and building natural frequency
ω_f	forcing frequency
ω_g	Kanai–Tajimi averaged natural frequency of near surface geology
Ω_g	ratio of Kanai–Tajimi averaged natural frequency of near surface geology to building natural frequency
ω_N	frequency parameter (nonlinear component of NTMD)
Ω_N	ratio of frequency parameter (nonlinear component of NTMD) and building natural frequency
Ω^*	value of Ω for which the linear TMD becomes optimal, $\Omega^* \approx 0.9215$.

There are many alternative approaches that have been advocated, such as isolating the structure from the ground motion, restricting the damage to sacrificial and replaceable elements, introduction of viscous/friction dampers, use of linear tuned mass dampers, etc. These alternate strategies seek to mitigate the seismic hazard without damaging the building structure in a way that will require a costly retrofit or rebuild.

This paper shall consider the tuned mass damper. The mechanics of the linear tuned mass damper (TMD) is well-known and extensively studied, even to the present [5–9]. A first problem encountered when employing a TMD is that it must be tuned to a particular modal frequency of the building, typically the first mode. Unfortunately, the building's natural frequency can change with time. This is due to changes in building use/occupancy that result in a variation of live load distribution and in changes to non-structural elements. These changes adjust the building's mass and stiffness that modify its modal frequencies. Correct tuning is vital for effective performance of a TMD and this is dependent on accurate knowledge of the building's natural

frequency. The second problem is that it is only effective over a narrow frequency bandwidth. Outside this frequency bandwidth it can be ineffective and possibly counter productive (depending on how it is tuned), that is, it can make the structure's response worse. Seismic ground motion normally has a broad frequency bandwidth. This critically undermines the effectiveness of employing a TMD in a building that is subject to a seismic event.

In this paper a nonlinear tuned mass damper (NTMD) is considered. This system was proposed in Ref. [15]. This follows on from the work on the energy pumping phenomenon in Ref. [16–19] and others. Ref. [19] provides a useful summary of historical papers in this field. It is suggested in Ref. [15] and by others that there are several advantages of the NTMD over the TMD namely (i) the proposed NTMD can be effective over a much broader range of frequencies than a linear TMD, (ii) the proposed NTMD does not suffer from the problem of amplification just outside the target bandwidth, (iii) the proposed NTMD requires smaller added mass than the TMD to be effective and (iv) the proposed NTMD is much more effective at reducing the transient vibrations at large amplitude than the TMD. However the complexity of the performance domain of the proposed NTMD was not fully explored. This is vital in the design of such a system in the real world. This paper shall more fully explore the performance of an NTMD when applied to a building that is subject to a seismic event. This exploration shall be undertaken using numerical continuation software commonly employed in the nonlinear dynamics community, Doedel et al. AUTO [10]; see also Refs. [11–14]. This is in contrast to various analytical approximations made in Refs. [15–19].

2. Equations of motion

2.1. Applying classical mechanics

The configuration of the NTMD is outlined in Fig. 1. It is composed of four springs, two acting in a geometric way to harden the system, and two acting in a linear way. Thus, it is a hardening Duffing oscillator [20,21]. There is no pre-stressing of these springs. An alternative design that follows [15] has only the two geometric springs that can be pre-stressed to introduce a linear spring stiffness term. However, the exact formulation is somewhat more complex (mathematically) than the one proposed here, because the coefficient of the linear and cubic stiffness terms are not independent of each another. Thus, Fig. 1 is conjectured as it allows more freedom to exploit the full range of parameters. The nonlinear elastic force f_s—deflection x relationship is

$$f_s = (2k_l)x + 2k_g x - \frac{2k_g L x}{\sqrt{L^2 + x^2}} \approx (2k_l)x + \left(\frac{k_g}{L^2}\right)x^3 + O(x^5), \tag{1}$$

which was shown to be approximately cubic within the scope of its intended use [15]. Its strain energy is

$$U_s = \frac{1}{2}k_2 x^2 + \frac{1}{4}k_N x^4, \quad k_2 = 2k_l, \quad k_N = \frac{k_g}{L^2}. \tag{2}$$

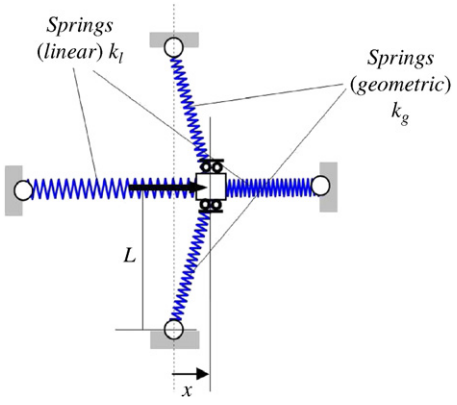

Fig. 1. Nonlinear tuned mass damper (NTMD).

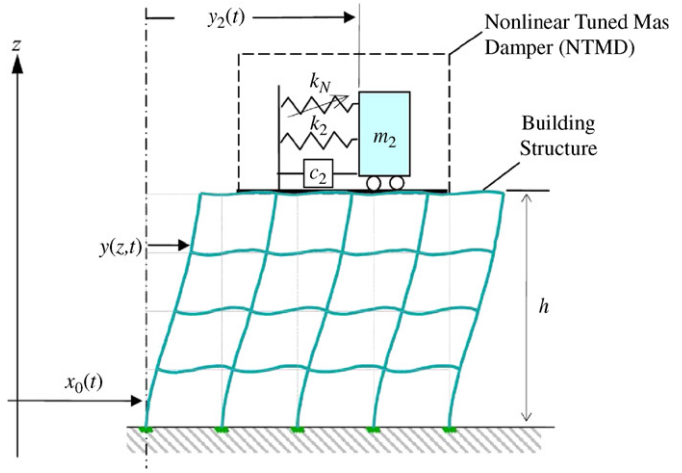

Fig. 2. Building structure with nonlinear tuned mass damper.

Consider a multi-story building with NTMD as sketched in Fig. 2. This building is subject to horizontal ground displacements $x_0(t)$. Assuming that the relative translational displacement of the building $y(z,t)$ can be expressed as the product of spatial and temporal functions $y(z,t) = y_1(t)\phi(z)$ we obtain a single mode and single degree of freedom representation of the building. Note that z is a normalized ordinate that equals one at the top of the building. The shape function $\phi(z)$ is normalized such that $\phi(1) = 1$. Hence, y_1 is the relative displacement of the top of the building.

The kinetic and potential energies and the Rayleigh dissipative function of the system are, respectively,

$$\begin{aligned} T &= \frac{1}{2}h\int_0^1 m(\dot{y}+\dot{x}_0)^2\,\mathrm{d}z + \frac{1}{2}m_2(\dot{y}_2+\dot{x}_0)^2 \\ &= \frac{1}{2}m_1\dot{y}_1^2 + m_{12}\dot{y}_1\dot{x}_0 + \frac{1}{2}m_{13}\dot{x}_0^2 + \frac{1}{2}m_2(\dot{y}_2+\dot{x}_0)^2, \end{aligned} \tag{3}$$

$$\begin{aligned} U &= \frac{1}{2}\frac{1}{h^3}\int_0^1 k_b y''^2\,\mathrm{d}z + \frac{1}{2}k_2(y_2-y(1,t)) + \frac{1}{4}k_N(y_2-y(1,t))^4 \\ &= \frac{1}{2}k_1y_1^2 + \frac{1}{2}k_2(y_2-y_1)^2 + \frac{1}{4}k_N(y_2-y_1)^4, \end{aligned} \tag{4}$$

$$\begin{aligned} R &= \frac{1}{2}h\int_0^1 c\dot{y}''^2\,\mathrm{d}z + \frac{1}{2}c_2(\dot{y}_2-\dot{y}(1,t))^2 \\ &= \frac{1}{2}c_1\dot{y}_1^2 + \frac{1}{2}c_2(\dot{y}_2-\dot{y}_1)^2, \end{aligned} \tag{5}$$

where

$$m_1 = h\int_0^1 m\phi^2\,\mathrm{d}z, \quad m_{12} = h\int_0^1 m\phi\,\mathrm{d}z, \quad m_{13} = h\int_0^1 m\,\mathrm{d}z, \tag{6}$$

$$c_1 = \frac{1}{h^3}\int_0^1 c\phi''^2\,\mathrm{d}z, \quad k_1 = \frac{1}{h^3}\int_0^1 k_b\phi''^2\,\mathrm{d}z. \tag{7}$$

The Euler–Lagrange equations of motion are:

$$\left.\begin{aligned} \ddot{x}_1 + 2\gamma_1\dot{x}_1 - 2\varepsilon\gamma_2\Omega(\dot{x}_2-\dot{x}_1) + x_1 - \alpha\varepsilon\Omega^2(x_2-x_1) - \varepsilon\Omega_N^2(x_2-x_1)^3 &= \rho\ddot{x}_0 + 2\gamma_1\dot{x}_0 + x_0, \\ \ddot{x}_2 + 2\gamma_2\Omega(\dot{x}_2-\dot{x}_1) + \alpha\Omega^2(x_2-x_1) + \Omega_N^2(x_2-x_1)^3 &= 0, \end{aligned}\right\} \tag{8}$$

which are stated in absolute coordinates $x_1 = y_1 + x_0$ and $x_2 = y_2 + x_0$ for simplicity. Note that we rescaled time to $\tau = \omega_1 t$. The equations of motion (8) contain a number of free parameters, which are related to design parameters via the relations (9)–(11).

$$\varepsilon = m_2/m_1, \omega_1^2 = k_1/m_1, \omega_N^2 = k_N/m_2, \omega_2^2 = k_2/m_2, \tag{9}$$

$$\gamma_1 = c_1/2\omega_1 m_1, \gamma_2 = c_2/2\omega_2 m_2, \Omega = \omega_2/\omega_1, \Omega_N = \omega_N/\omega_1, \tag{10}$$

$$\rho = 1 - m_2/m_1, \tau = \omega_1 t. \tag{11}$$

The differences between Eqs. (8) and Eqs. (3) in Ref. [15] are twofold. Firstly, a linear stiffness term is included for the attached NTMD. This was absent in Eq. (3) in Ref. [15]. Thus, the aim is to fully explore the role of this linear spring term as well as the cubic spring stiffness term. The second difference is a subtle one, the linear damping of the NTMD is here a function of the frequency parameter Ω. In Ref. [15] the linear damping term was assumed to be independent of Ω. The rationale in employing a constant damping coefficient term with respect to frequency in Ref. [15] was pragmatic as the experimental tests were performed on a model with a fixed geometry. However, here a more general study is performed and it is likely that a constant ratio of critical damping may be targeted by a designer rather than a constant damping coefficient as in Ref. [15]. In order to have Eq. (3) in Ref. [15] as a special case of Eq. (8) here, we introduced the parameter $\alpha \in \{0, 1\}$. If we set $\alpha = 0$ we can directly relate the parameters between the two model equations. If we set $\alpha = 1$ we can perform calculations for our more realistic model. For the majority of our computations we use $\alpha = 1$.

2.2. Idealized ground motion

In order to perform a full parametric continuation of all solutions of the nonlinear system it is expedient to assume that the ground motion has the form

$$x_0 = \beta(\omega)\sin(\omega\tau + \xi), \quad \omega = \omega_f/\omega_1, \tag{12}$$

where ω_f is the forcing frequency and ω is the forcing frequency to building structure frequency ratio. This monochromatic form is clearly not an exact substitute for an earthquake. However, if $\beta(\omega)$ is proportional to the power spectrum of a typical earthquake time history it can be viewed as a coarse first approximation. This $\beta(\omega)$ is chosen such that Eq. (12) provides the same total power to the nonlinear system as a design earthquake.

Kanai [22] and Tajimi [23] proposed a smoothed power spectrum estimate for ground displacement time histories; this is described in Ref. [24]. We follow this approach and use the frequency-dependent forcing amplitude

$$\beta(\omega) = AH_{\mathrm{kt}}(\omega), \quad H_{\mathrm{kt}}(\omega)^2 = \frac{G_0\left(1 + (2\gamma_g(\omega/\Omega_g))^2\right)}{\left(1 - (\omega/\Omega_g)^2\right)^2 + \left(2\gamma_g(\omega/\Omega_g)\right)^2}, \tag{13}$$

in all our computations, where $\Omega_g = \omega_g/\omega_1$. Here, we included the amplitude parameter A to allow a variation in the event magnitude. The function H_{kt} is effectively the linear single degree of freedom transfer function for the soil layer below the structural foundations (often termed the near surface geology); where ω_g and γ_g are its natural frequency and ratio of critical damping.

2.3. Physical interpretation of forcing parameter A

The Kanai–Tajimi spectrum is a power spectrum (in the *Fourier* frequency domain) rather than in the time domain. This raises the question of how should the forcing parameter be interpreted when applied in the time-domain.

Assume that the monochromatic sinusoidal function $x_0(\tau)$ has a finite duration of D seconds. The total intensity (power) of $x_0(\tau)$ is

$$I_x = (AH_{\mathrm{kt}}(\omega))^2 \int_0^D \sin(\omega\tau)^2 \,\mathrm{d}\tau = \frac{1}{2}(AH_{\mathrm{kt}}(\omega))^2 D. \tag{14}$$

Assuming that $D = 2\pi n/\omega$, where $n \in \mathbb{N}$, the total power of the Kanai–Tajimi event is then

$$I_{\mathrm{kt}} = \int_{-\infty}^{\infty} |H_{\mathrm{kt}}(\omega)|^2 \,\mathrm{d}\omega = \frac{\pi G_0 \Omega_g (1 + 4\gamma_g^2)}{2\gamma_g}. \tag{15}$$

If the total intensity of the Kanai–Tajimi event is expressed in the monochromatic sinusoidal function then by Parseval's theorem $I_x = I_{\mathrm{kt}}$, hence,

$$A_e = \frac{1}{H_{\mathrm{kt}}(\omega)} \sqrt{\frac{\pi G_0 \Omega_g (1 + 4\gamma_g^2)}{\gamma_g D}}. \tag{16}$$

Subsequently, in this paper, parameter A is used as a variable for parametric continuation. When $A = A_e$ (obtained from Eq. (16)) the total intensity of the forcing function equals the total intensity of the Kanai–Tajimi event.

The graphical representation of Eq. (16) is given in Fig. 3. The minimum of A_e occurs at $\omega_f \approx 0.91\omega_g$ which is the resonance condition of the soil/rock column that is below the structure itself. In this case the minimum value is $A_e = 2.33$, though it should be pointed out that this is a function of the Kanai–Tajimi parameters employed in this example. Thus, at or about the linear resonance condition of the structure, that is, $\omega \approx 1$, the value of A_e is somewhere between 2.33 and 4.27.

2.4. Final form of equations of motion

Using the monochromatic ground displacement $x_0(\tau)$ as above we obtain $\rho\ddot{x}_0 + 2\gamma_1\dot{x}_0 + x_0 = F(\omega)\sin(\omega\tau)$ as the right-hand side of Eq. (8). Thus, the forcing amplitude term F becomes

$$F(\omega) = AH_{\mathrm{kt}}(\omega)H_s(\omega), \tag{17}$$

where $H_s(\omega)$ is the support/building transfer function

$$(H_s(\omega))^2 = (1 - \rho\omega^2)^2 + (2\gamma_1\omega)^2. \tag{18}$$

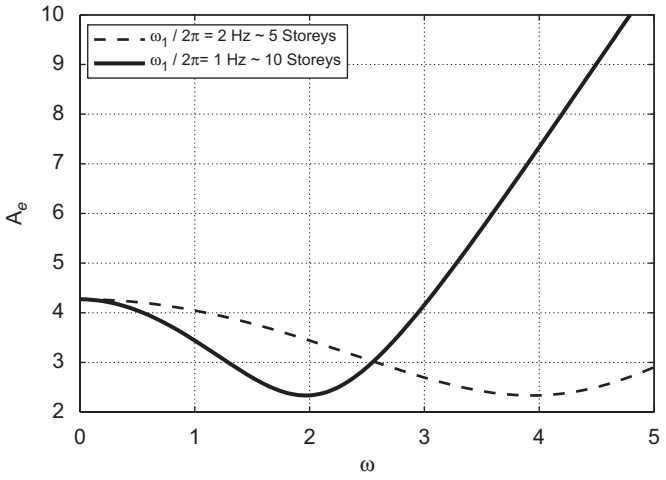

Fig. 3. Example of variation of A_e vs. forcing frequency ratio ω for a range of structures ω_1. Kanai–Tajimi parameters: rock site $G_0 = 0.07$, $\omega_g = 27$, $\gamma_g = 0.34$, $D = 20$ s.

We combine Eqs. (13), (17), (18) and (8) to obtain the final form of the system of equations

$$\left.\begin{aligned} \ddot{x}_1 + 2\gamma_1\dot{x}_1 - 2\varepsilon\gamma_2\Omega(\dot{x}_2 - \dot{x}_1) + x_1 - \alpha\varepsilon\Omega^2(x_2 - x_1) - \varepsilon\Omega_N^2(x_2 - x_1)^3 &= F(\omega)\sin(\omega\tau), \\ \ddot{x}_2 + 2\gamma_2\Omega(\dot{x}_2 - \dot{x}_1) + \alpha\Omega^2(x_2 - x_1) + \Omega_N^2(x_2 - x_1)^3 &= 0. \end{aligned}\right\} \tag{19}$$

The forcing parameters are amplitude A and frequency ratio ω .

3. Computational analysis

3.1. Preliminaries

All numerical computations were performed with AUTO [10] and the figures were drawn with gnuplot [25] and MATLAB [26]. In our study, we are concerned with finding design parameters of an NTMD for which the building has low-amplitude responses over a wide range of forcing frequencies. We consider the worst-case scenario that the structure's first mode frequency coincides with the frequency at which the ground motion of an Kanai–Tajimi event has its largest amplitude. For simplicity we use the model equations (19) exactly as stated, even though x_1 and x_2 include the ground motion. Although this does lead to a slight shift in the amplitudes of the responses, the qualitative features we are looking for remain the same.

Due to the complexity of the system a range of output measures are employed for emphasizing specific aspects of our model. Most commonly we use the L_2 norm

$$\|x_1\|_2^2 = \frac{1}{T}\int_0^T x_1(\tau)^2\,\mathrm{d}\tau \tag{20}$$

of an individual generalized coordinate over one period T as a measure of the response amplitude. This norm can be interpreted as a 'generalized amplitude' and is identical to the amplitude for harmonic oscillations. However, its definition carries over to general oscillations, which we will encounter in NTMDs. For comparison we sometimes show the absolute maximum response amplitude, which is given by the supremum norm

$$\|x_1\|_\infty = \max_{t\in[0,T]} |x_1(t)| \tag{21}$$

over one period. Some details of our results are best represented using the L_2 norm

$$\|u\|_2^2 = \|x_1\|_2^2 + \|\dot{x}_1\|_2^2 + \|x_2\|_2^2 + \|\dot{x}_2\|_2^2 \tag{22}$$

over the full solution vector over one period. For the most part, in the present study $\|u\|_2$ is good for showing coexistence of solutions. The measure $\|x_1\|_2$ is used for optimizations because the designer is mainly interested in the response of the building structure and it is a smooth function of the system's parameters. Furthermore, it behaves very similar to $\|x_1\|_\infty$, which is conventionally what a designer wants to minimize. We give evidence for these claims in Figs. 6 and 7.

System (19) has a four-dimensional phase space when stroboscopic Poincaré sampling ($\tau \in [2\pi n/\omega : n \in \mathbb{N}]$) is employed. It has seven system parameters: the structural parameters Ω, Ω_N, γ_1, γ_2, ε and the forcing parameters A and ω. Clearly, an exhaustive exploration of this high-dimensional parameter and phase space is a challenge. This is especially the case when graphical representations are required for interpretation. In this paper, the influence of damping parameters is not explored. Thus, we fix the structure's damping ratio at $\gamma_1 = 0.02$, which is a typical value for a steel framed structure that undergoes no inelastic behavior [27]. We set the NTMD's damping ratio as high as could be achieved without any specialized viscous damper that would require maintenance, that is, $\gamma_2 = 0.05$. We keep the mass ratio of added mass to structural mass constant at $\varepsilon = 0.1$. This is the largest value that we assume to be feasible as the static capacity of the structure is limited. We study families of frequency response curves for which we vary the forcing amplitude in $A \in [0, 5]$ and the forcing frequency in $\omega \in [0, 5]$.

3.2. Effect of the frequency-dependent forcing amplitude $F(\omega)$

For a purely mathematical investigation one would use the constant amplitude forcing term $F(\omega) = f$, which is much simpler to deal with than the forcing term in Eq. (19). However, a close look at the forcing term reveals that, compared with constant forcing, the proposed forcing is merely a coordinate transformation in parameter space. That is, the qualitative properties of the equation under investigation do not change, but the quantitative properties, like response amplitudes, will be different. The aim here is a parameter study that provides useful information for designing a nonlinear tuned mass damper for the purpose of reducing vibrations of buildings during earthquakes. As a frequency-dependent forcing might influence design decisions it is taken into account. Furthermore, since we use numerical rather than analytical methods the more complicated forcing term does not impose any restriction to our subsequent investigations.

This interpretation, that a frequency-dependent forcing amplitude can be viewed as a change of coordinates in parameter space is illustrated in Figs. 4 and 5 . Fig. 4 shows the amplitude of ground motion in meters of an event with event magnitude $A = 1$ according to the Kanai–Tajimi spectrum. Since the forcing term in Eq. (19) contains only the two parameters event magnitude A and forcing frequency ω, only these two parameters are affected by the transformation—all other parameters keep their original meaning. Fig. 5 shows the constant-A coordinate lines of the transformation $(\omega, A) \leftrightarrow (\omega, F)$ in the (ω, F)-parameter plane. They are slightly different from horizontal lines, which would represent constant forcing. This frequency dependence will lead to a change of shape of frequency–response curves compared with those for constant forcing. Note the peak around the normalized resonance frequency $\omega = 1$. We will observe quantitative differences in this important range of frequencies.

To get a first impression of what influence the variable forcing term has, the well-known frequency response function of a linear tuned mass damper is computed; see Fig. 6. For this computation we chose the model parameters $A = 1$, $\Omega_N = 0$, $\varepsilon = 0.1$, $\gamma_1 = 0.02$ and $\gamma_2 = 0.05$ and computed the responses for $\omega = 0.2 \ldots 1.8$ and $\Omega = 0.2 \ldots 1.8$. Fig. 6 shows two different visualizations of the results. Fig. 6a is a surface plot of the amplitude of the primary structure as a function of the two parameters ω and Ω. Observe the 'valley of suppression' of the oscillations of the primary structure. Fig. 6b is an intensity plot in logarithmic scale. Higher amplitudes correspond to darker shading as indicated with the color bar. The main difference to the traditional result (obtained with constant forcing amplitude) is that the gradient of the surface in Fig. 6a is much steeper close to the resonance frequency $\omega = 1$. Fig. 6c shows a comparison of the structure's response

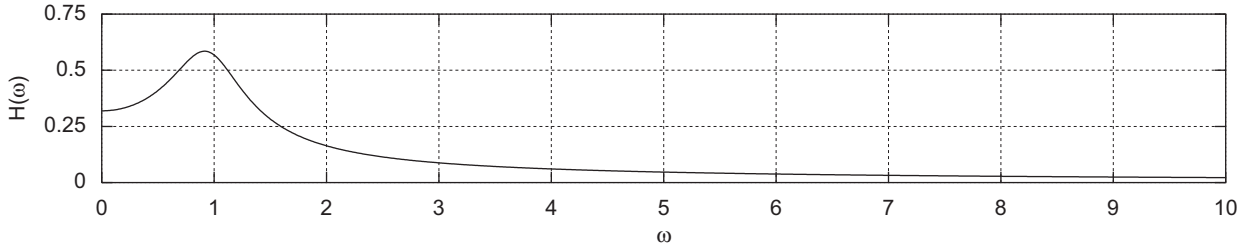

Fig. 4. Amplitude of ground motion depending on the frequency for the Kanai–Tajimi spectrum with an event magnitude of $A = 1$.

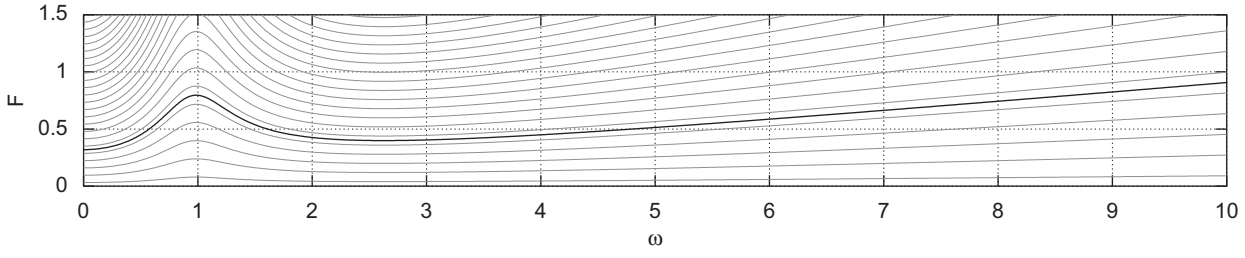

Fig. 5. The frequency-dependent forcing amplitude is equivalent to a coordinate transformation in the (ω, F) parameter plane. The curve with event magnitude $A = 1$ is emphasized.

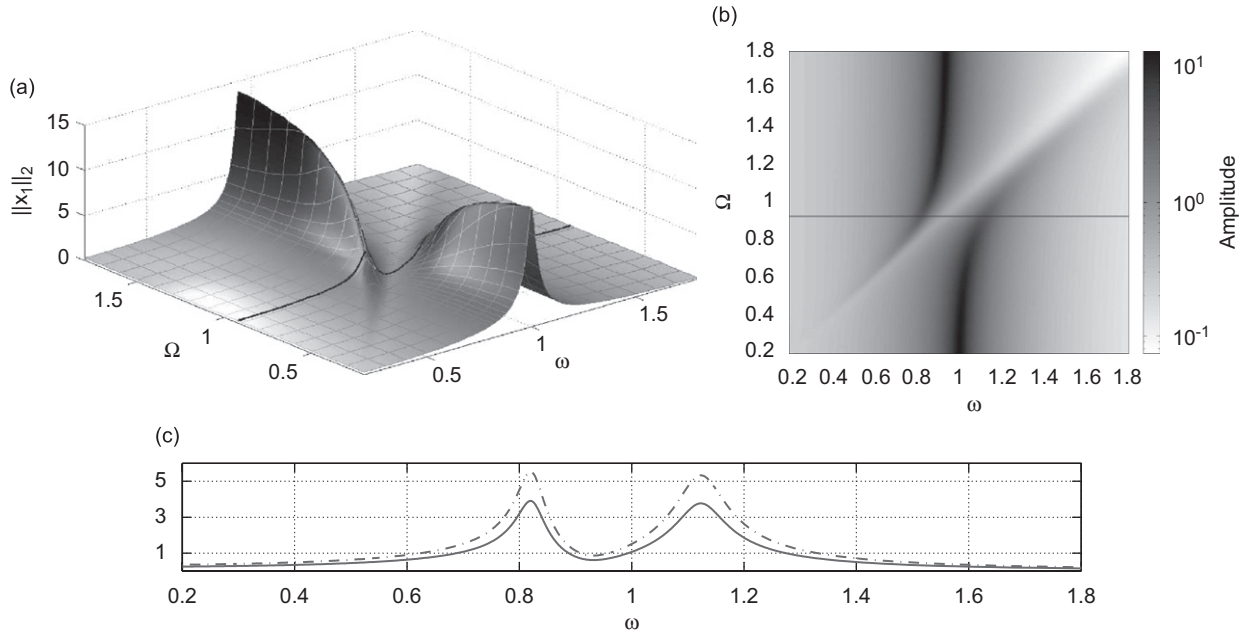

Fig. 6. Surface plot (a) and intensity plot (b) of the frequency–response function of the primary structure for different design parameters Ω of a linear TMD for event magnitude $A = 1$. Panel (c) shows the frequency response curve for $\Omega = 0.925$, which is nearly optimal and highlighted as a black curve in panels (a) and (b). The solid curve is $\|x_1\|_2$ and the dash-dot curve is $\|x_1\|_\infty$.

for a nearly optimal TMD, illustrating that the qualitative behavior of the supremum and the L_2 norm are similar.

3.3. Initial parameter continuation sweeps

As an initial investigation two parameter sweeps were performed: (i) The left-hand column in Fig. 7 is a frequency sweep for varying forcing frequency ω and fixed forcing amplitude A of the fundamental period-1 solutions. (ii) The right-hand column of this figure is an amplitude sweep at fixed frequency. The line type indicates stability: solid lines denote stable periodic solutions and dotted lines denote unstable ones. Our notation follows the AUTO [10] classifications: a diamond marks a limit point (LP) or saddle-node bifurcation point and a circle marks a torus (TR) or Neimark–Sacker bifurcation point. Note again that Figs. 7(b), (c), and (e), (f), show that the amplitude measure L_2 norm is qualitatively similar to the supremum norm.

To explain these figures, consider what happens to the two resonance peaks of the linear TMD system as sketched in Fig. 8. As we activate and increase the nonlinearity while decreasing the linear spring stiffness to zero, the higher-frequency resonant peak drops and bends towards the higher frequencies; see Fig. 8(b). This is a classical feature of a hardening spring system. A torus bifurcation and a saddle-node bifurcation act independently to limit and reduce the amplitude of this resonance peak. In this regime the energy of the periodic response oscillations is mainly transferred from the structure to the NTMD. This is excellent in terms of reducing the amplitude of the structure's response.

However, in the process of this parameter change the lower-frequency resonant peak gains amplitude and *detaches* from the continued path of the higher frequency resonance. This is what we observe in Fig. 7(a) and is an important feature of the frequency response curve. Unfortunately, this behavior is not necessarily picked up by employing a harmonic balance method. An asymptotic analysis, as carried out in Ref. [15], finds the small-amplitude responses locally connected to the solution $u = 0$ for $A = 0$. These are the solutions on the lower branch of the response curve, but not necessarily *all* responses. In fact, even with numerical continuation it is easy to miss this feature. We discovered it only after a substantial number of further frequency sweeps at different A values, whereby we obtained the complete response surface with respect to A and ω shown in

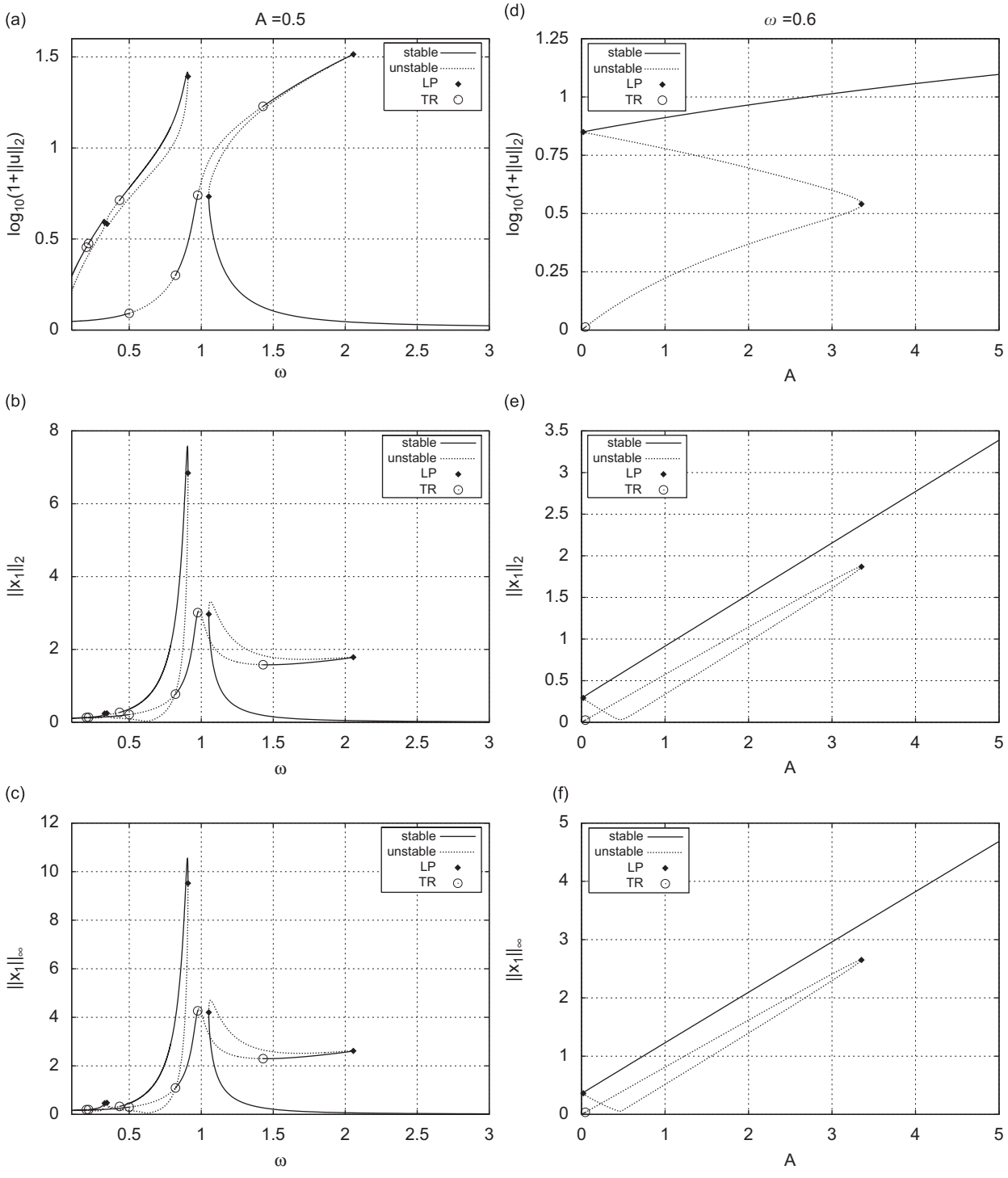

Fig. 7. Bifurcation diagrams of the response curves highlighted in Fig. 9 using different amplitude measures. Observe the *detached response curve* best visible in panel (a). Parameters: $\Omega = 0$, $\Omega_N = 0.1$, $\varepsilon = 0.1$, $\gamma_1 = 0.02$, $\gamma_2 = 0.05$. Notation: LP is a limit point (saddle-node bifurcation) and TR is a torus (Neimark–Sacker) bifurcation. Panels (a) to (c) are continuation plots showing different amplitude measures of the response curves as a function of the forcing frequency. Similarly, panels (d)–(f) show the same amplitude measures as a function of the forcing amplitude.

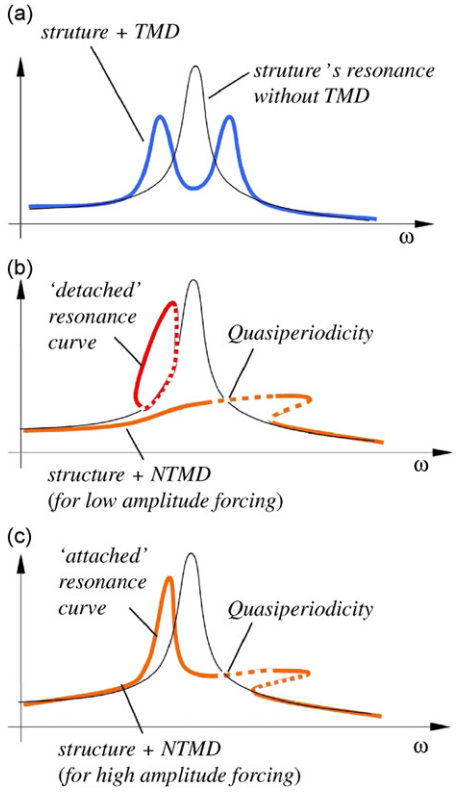

Fig. 8. Schematic comparison of TMD and NTMD (without linear stiffness term as in Ref. [15]). The response of the primary structure alone is compared with (a) TMD attached, (b) NTMD attached (low forcing amplitude) and (c) NTMD attached (high forcing amplitude).

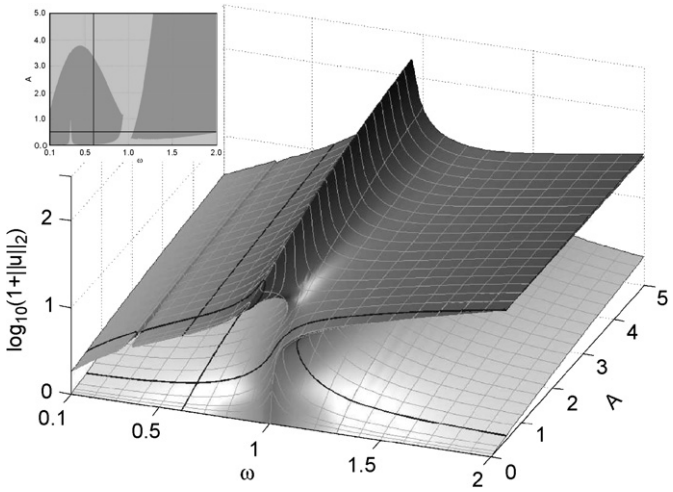

Fig. 9. Three-dimensional nonlinear response surface for $\Omega = 0$, $\Omega_N = 0.1$, $\varepsilon = 0.1$. The thumbnail picture in the top-left corner illustrates the domains of coexistence of several response solutions. In the light gray areas there exists at least one and in the dark gray areas there exist at least three solutions. The black lines on the surface are response curves shown in detail in Fig. 7.

Fig. 9. At $A = 0.5$ it appears that the lower resonance response curve is *detached* from the higher resonance response curve. This figure also shows that all these responses are part of some continuous response surface that is now a multivalued function (manifold). Note that for higher forcing amplitudes the detached responses reconnect as illustrated in Fig. 8(c).

In our subsequent study, we explore the influence of the nonlinear and linear spring stiffnesses over a large range of values. The aim is to determine whether it is possible to design the dynamics of the system such that we can eliminate this lower-frequency resonance peak in some way as well.

3.4. Exploring local extrema

In our proposed NTMD design we have two fundamental system parameters, the linear and the nonlinear spring stiffness while a TMD has only one. Given this additional freedom to design an NTMD a first question that springs immediately to mind is: is it possible to tune the two spring stiffnesses in such a way that an NTMD will always outperform a TMD? In order to tackle this problem we use an advanced feature of the continuation package AUTO [10], namely, the optimization of periodic solutions. Starting with a periodic solution that has an extrema with respect to some objective function one can successively add free parameters and continue extremal periodic solutions. In our case we choose the L_2 norm $\|x_1\|_2$ as the objective function, that is, we look for periodic responses with extremal amplitudes. Our ultimate goal is to find a set of spring stiffnesses for which all extremal solutions have amplitudes below the peaks of a TMD, leading to an NTMD that is superior to an optimal TMD.

To start our investigation we need to find a set of suitable start solutions. We have already seen that the frequency response curves we deal with are quite complicated. To make sure we do not overlook an important branch of solutions we performed a couple of parameter sweeps for $A = 1$, $\varepsilon = 0.1$, optimal linear spring stiffness $\Omega = 0.9215 \approx \Omega^*$ and some nonlinear spring stiffnesses $\Omega_N \in [0, 5]$. After reviewing the results we picked the curve for $\Omega_N = 3.0$, which gave seven start solutions; see Fig. 10a. The large dots signify the locations of the local extrema with respect to forcing frequency ratio ω. Our aim is to produce a diagram that

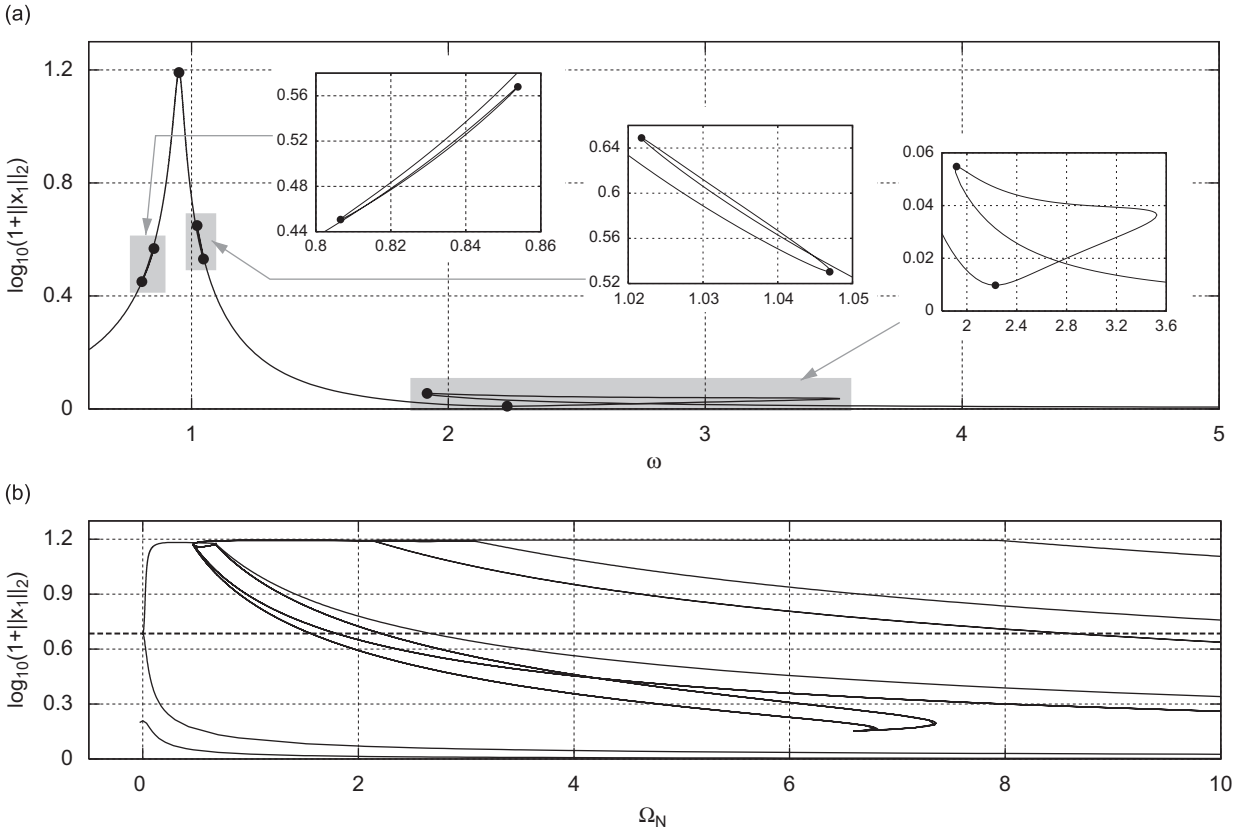

Fig. 10. (a) Extrema of the nonlinear response curve for $\Omega = 0.9215 \approx \Omega^*$, $\Omega_N = 3.0$, $A = 1$, $\varepsilon = 0.1$. (b) Continuation of these extrema with respect to Ω_N and ω. The horizontal dashed line indicates the performance of an optimal TMD.

shows all extremal solutions as functions of Ω and Ω_N. Hence, we initiated a first continuation of these seven extremal solutions with respect to the two parameters Ω_N and ω. The result is shown in Fig. 10b. The dashed horizontal line shows the maximum responses for an optimal TMD.

Starting with points along the curves shown in Fig. 10b we initiated a large number of continuations of these extrema for selected but fixed values $\Omega_N \in [0, 10]$ with respect to the linear spring stiffness $\Omega \in [0, 2]$. These results are not shown here, because they are always the same: No matter what value of Ω we chose, adding the slightest amount of nonlinearity to the system leads to high-amplitude responses in the same way as shown in Fig. 10b. This suggests that it is not possible to bound all responses of an NTMD below the maximum responses of a linear TMD by adjusting either Ω_N and/or Ω.

This result seems quite discouraging. However, it should be pointed out that these computations try to employ a very strong property, namely, to bound *all responses* of an NTMD. We do not consider stability and, indeed, we are mainly interested in bounding *stable responses*. Hence, the above investigation should be considered as a first pass at exploring the problem domain. In a next step we need to include stability. In other words, we consider the question: is it possible to use the nonlinearity to destabilize the high-amplitude responses and design an improved NTMD?

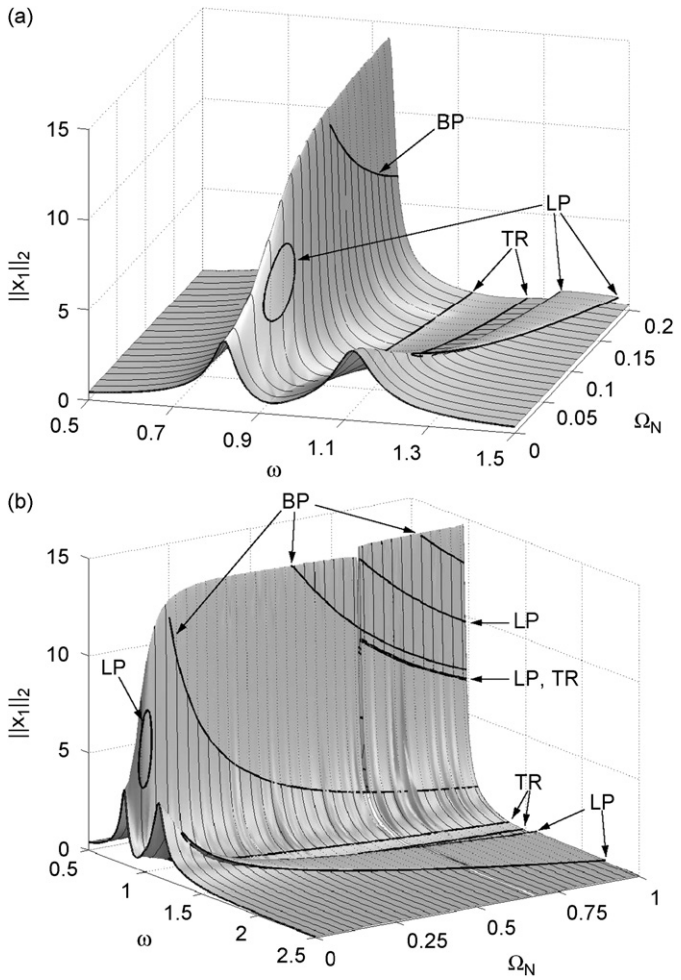

Fig. 11. Three-dimensional bifurcation diagrams illustrating the effect of the nonlinear spring in more detail for $\Omega = 0.9215 \approx \Omega^*$, $A = 1$, $\varepsilon = 0.1$. Notation: LP is a locus of limit points (saddle-node bifurcations), BP of bifurcation points (pitchfork) and TR of torus (Neimark–Sacker) bifurcations. Panel (a) is an enlargement of panel (b) that focuses on smaller nonlinear spring stiffnesses parameter Ω_N.

3.5. Further studies on response surfaces

As observed in the previous section it seems impossible to find parameter values for which the amplitudes of all response solutions, including the unstable ones are smaller than those of a linear TMD. Therefore, we are going to conduct an investigation into the stability of these response solutions. The idea is to look for parameter values for which the large-amplitude responses become unstable and the remaining stable responses have low amplitude. To this end, we perform a number of *scans*, that is, we execute a large number of similar continuations with respect to ω, where a second parameter is slowly incremented to *scan* a two-parameter plane.

This procedure is illustrated in Fig. 11, which shows two different views on the same response surface for $\Omega = \Omega^* \approx 0.9215$; Fig. 11a is an enlargement of Fig. 11b. For $\Omega_N = 0$ we find the response curve of the classical optimal TMD; *cf*. Fig. 6. As we add nonlinearity to the system by increasing Ω_N we observe that the high-frequency resonance peek becomes suppressed, while the amplitude of the low-frequency resonance peak

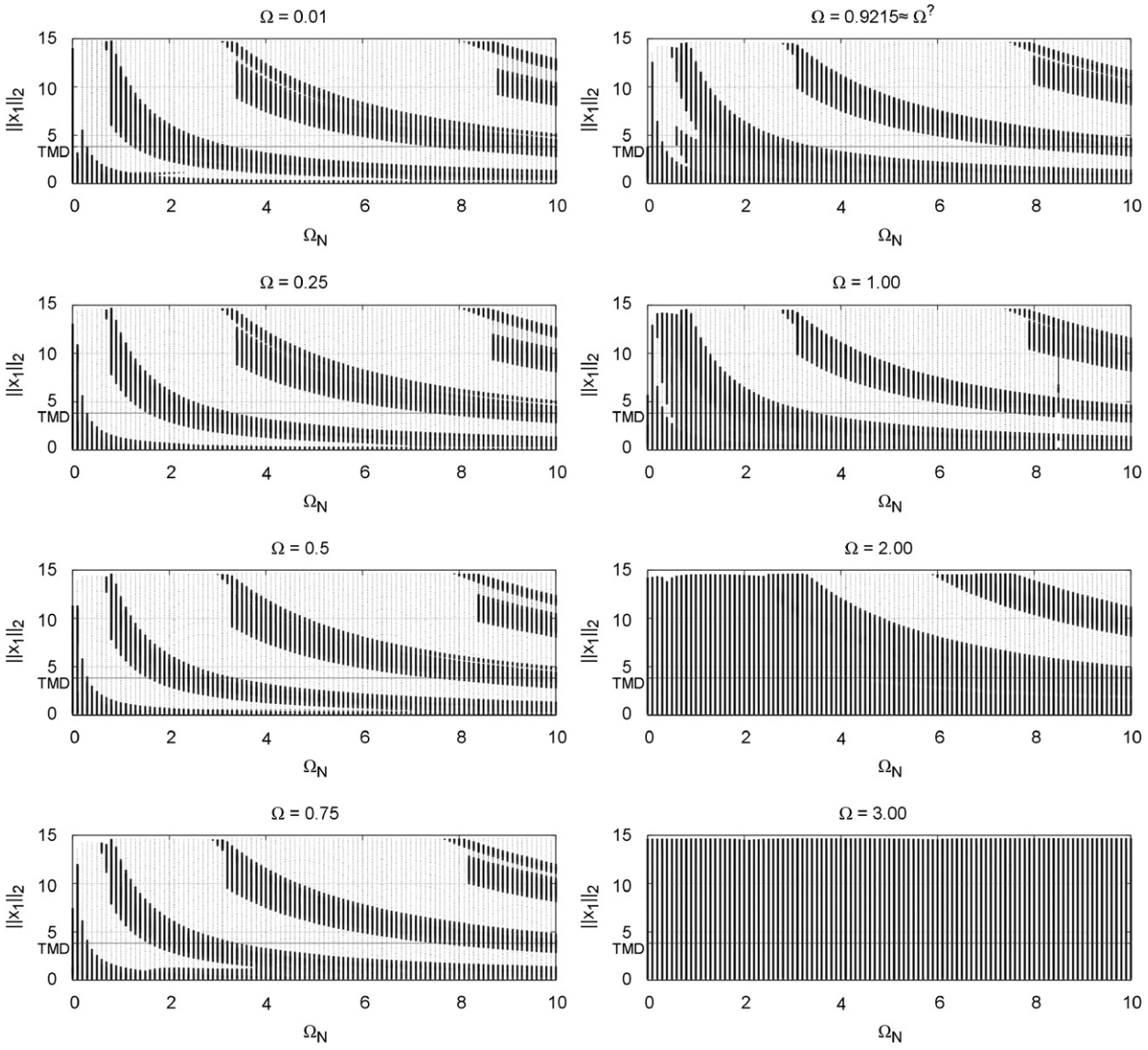

Fig. 12. Projections of the response surfaces along the ω-axis for different Ω with respect to Ω_N. Parameters: $A = 1$, $\varepsilon = 0.1$, $\omega \in [0, 5]$.

grows dramatically. However, we also observe changes in stability as indicated by the line style of the response curves plotted on the surface; solid marks stable and dashed unstable responses. Namely, we find a 'window of instability' for $\Omega_N \approx 0.1 \ldots 0.5$ inside which the high-amplitude responses become unstable in a Pitchfork bifurcation (BP for branch point). Thus, there might be a chance to find parameter regimes with the property that the responses on the lower-frequency resonance peak are unstable and the remaining stable responses have low amplitude.

To gain as much of an overview as possible we performed a number of scans in Ω over an extended range $\Omega_N \in [0, 10]$ for different linear spring stiffnesses Ω as shown in Fig. 12. At this point we have to make an important remark. While it is possible to perform scans which numerically analyze the primary period-one responses in an automated way with AUTO [10], it is not possible to include bifurcating responses. Hence, the scans we executed are a first step only and one should use the computed information merely as a guide to *exclude* parameter ranges of unfavorable dynamics and continue the investigation with the remaining regions. The graphs in Fig. 12 show a projection of the response surfaces onto the (response amplitude)–(nonlinear stiffness) parameter plane. One can consider this as viewing the three-dimensional response surface shown in Fig. 11 along the forcing frequency ratio ω-axis, the surface being transparent. Hence, the thick solid lines show areas where at least one stable response exists, and the thin dotted line areas where no stable responses exist on the primary period-one branch.

We find that '*bands of stability*' seem to sweep down from top left to bottom right for increasing Ω_N. A structure similar to these 'bands of stability' is also present in Fig. 10b. As a guide for comparison we indicated the performance of the linear TMD with a horizontal line. The figures in the right-hand column show that for values of linear stiffnesses $\Omega \geqslant \Omega^*$ there always exist stable responses that have amplitudes larger than TMD responses. For linear stiffnesses $\Omega < \Omega^*$ we find a gap for $\Omega_N \approx 0.3 \ldots 0.7$ where all stable period-one responses have amplitudes less than the TMD responses.

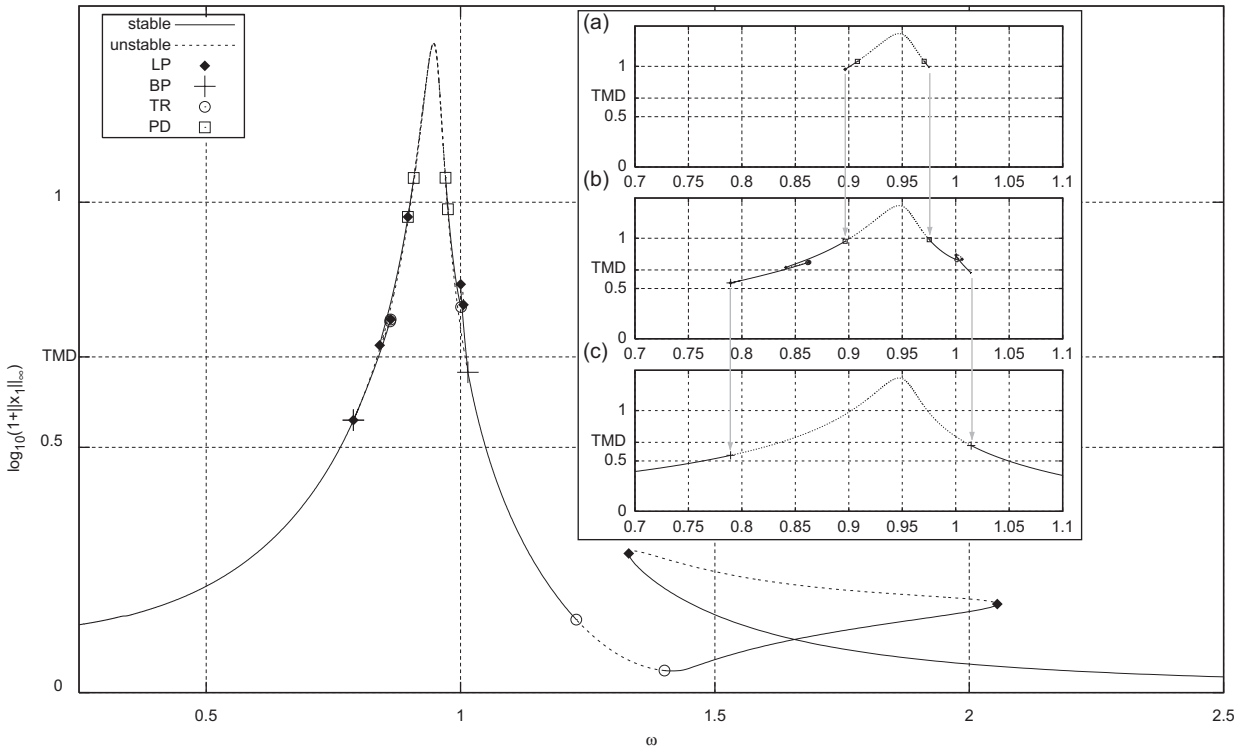

Fig. 13. Nonlinear response curves for $\Omega_N = 0.5$, $\Omega = 0.25$, $A = 1$ and $\varepsilon = 0.1$. This diagram is a superposition of several branches of responses emerging from bifurcation points as indicated in the panels (a)–(c). Notation: LP is a limit point (saddle-node bifurcation), BP is a bifurcation point (pitchfork), PD is a period-doubling point and TR is a torus (Neimark–Sacker) bifurcation.

We continue our investigation with parameters inside this window of opportunity, namely, $\Omega = 0.25$ and $\Omega_N = 0.5$. We recomputed the primary branch of period-one responses and this time followed the bifurcating solutions; see Fig. 13. Unfortunately, what we find is that the amplitudes of these stable solutions are not bounded below the TMD line. This is illustrated in more detail in Figs. 13(a)–(c). Panel (c) shows a zoom-in on the primary branch of period-one responses, which become unstable in a Pitchfork bifurcation. Panel (b) shows the branch of bifurcating solutions. These become unstable in a period-doubling bifurcation and the emanating branch is shown in panel (a). Note that the stable responses in panels (a) and (b) have amplitudes well above the TMD line.

The presence of these stable responses has also been confirmed in time–history simulations. From these results we have to conclude that stable large amplitude responses exist even in the best parameter window. Thus, it seems unlikely that one can design an NTMD with cubic and linear stiffness terms that would outperform an optimal TMD.

4. Discussion and conclusions

It seems highly improbable that the proposed NTMD can generally outperform a TMD, regardless of the parameters adopted. In this paper a full parametric investigation was made into the influence of the linear springs and geometric springs (cubic stiffness term).

The conclusion of the numerical studies in this paper seem to contradict work presented in Ref. [15]. As the the analysis in Ref. [15] was based on experimental and theoretical approaches an explanation is required. The systems analyzed in Ref. [15] and here differ in two respects. Firstly, Ref. [15] investigated a system without the presence of the linear springs or pre-stress in the geometric springs, that is, with no linear stiffness terms. Secondly, a constant damping coefficient was adopted rather than a constant damping ratio as we did here. While these differences are important they are not sufficient to explain the discrepancies in the findings. We used a system identical to Ref. [15] for direct comparisons. In these direct comparisons between the results obtained in Ref. [15] using the harmonic balance method (Fig. 17 in Ref. [15]) and the computational results produced with AUTO (Figs. 7–9) it appears that the *detached resonance curve* was undetected in Ref. [15]. Thus, considering the lower sheet of the response surface, it does seem that the NTMD outperforms the TMD. It was unfortunate that experimental work did not identify this feature. Further experimental work with different initial conditions might have picked this up.

A full investigation of the initial conditions that are attracted to the lower and upper sheet has not been undertaken here. This requires the development of a strategy for extending the work on two-dimensional catchment basins (Ref. [28–31]) to higher-dimensional phase spaces. This is not difficult but it is computational expensive. Also, it does pose the challenge of graphically representing catchment basins that are hyper-volumes in $\mathbb{R}^4$. This is beyond the scope of this paper, but would be very useful to perform in the future, because there might be a possibility to manipulate the catchment basins in some way. Such an investigation could be a starting point for designing semi-active NTMDs.

An intention for introducing the linear springs (linear stiffness terms) was to remove the *detached resonance curve* feature in order to obtain a simpler regime in parameter space that still shows good system performance. It did achieve a removal of this feature. However, after extensive searches of the higher-dimensional parameter space $\mathbb{R}^7$ it appears that there are no good choices of system parameters that lead to an NTMD that is superior to a linear TMD.

The conclusions are negative, as a *passive device*, the proposed NTMD in any configuration will generally not provide an improvement over an optimal linear TMD. From an engineering point of view the cubic hardening nonlinearity reduces only the amplitude of the higher-frequency resonance. This is achieved by bending it towards the higher frequencies. However, regardless of the choice of parameters it seems impossible to limit the response amplitude of the lower-frequency resonance peak.

The presence of a *detached resonance curve* is identified in the contemporaneous paper [32]; where the authors attach an NTMD (again without linear stiffness terms) to a two degree of freedom linear structure. In a sense we have attached the NTMD to a particular linear mode of a multi-degree of freedom building. The method employed in Ref. [32] is complex-averaging approach that is an analytical approximation. These approximations show much of the bifurcation structures observed by employing numerical continuation and

support our findings reported here. They also indicate that the *detached resonance curve* is a structurally stable feature in the sense that its occurrence seems independent of the number of modes used for approximations. These investigations contrast with the harmonic balance and multi-timescales analytical approximations employed in Ref. [15] that did not identify the *detached resonance curve*.

It may be possible to view the *detached resonance curve* feature in a positive light. As the system has coexisting stable solutions within this range of frequencies, it may be possible to encourage the system to be attracted to the lower-amplitude responses. There seems to be an opportunity for smart semi-active control. It might be possible that the application of small forces, carefully timed, destabilizes the higher-amplitude solutions in the *detached resonance curve*. Thus, while the presence of the *detached resonance* is a weakness of the NTMD (with solely cubic stiffness terms) it may provide an opportunity for constructing *semi-active NTMDs*.

Acknowledgments

FS was supported by EPSRC Grants GR/R72020/01 and EP/D063906/1.

References

[1] A.K. Chopra, *Dynamics of Structures, Theory and Applications to Earthquake Engineering*, second ed., Prentice-Hall, Englewood Cliffs, NJ, 2000.
[2] International Code Council, International Building Code (IBC), Falls Church, VA, 2000.
[3] E. Miranda, V.V. Bertero, Evaluating strength reduction factors for earthquake resistant design, *Earthquake Spectra* 10 (2) (1994) 357–379.
[4] J. Garamendi (Commissioner), Press release on *Eve of Northridge Earthquake's 10th Anniversary, Cautions of Huge Risk as More Californians Decline Earthquake Insurance*, California Department of Insurance, USA, January 16, 2004.
[5] J.P. Den-Hartog, *Mechanical Vibration*, McGraw-Hill, New York, 1947.
[6] R. Villaverde, Reduction in seismic response with heavily-damped vibration absorbers, *Earthquake Engineering and Structural Dynamics* 13 (1985) 33–42.
[7] F. Sadek, B. Mohraz, A.W. Taylor, R.M. Chung, Method of estimating the parameters of tuned mass dampers for seismic applications, *Earthquake Engineering and Structural Dynamics* 26 (1997) 617–635.
[8] J.C. Miranda, On tuned mass dampers for reducing the seismic response of structures, *Earthquake Engineering and Structural Dynamics* 34 (2005) 847–865.
[9] G. Chen, J. Wu, Experimental study on multiple tuned mass dampers to reduce seismic responses of a three-storey building structure, *Earthquake Engineering and Structural Dynamics* 32 (2003) 793–810.
[10] E. J. Doedel, A. R. Champneys, Th. F. Fairgrieve, Y. A. Kuznetsov, B. Sandstede, X. Wang, *AUTO 97*: *Continuation and Bifurcation Software for Ordinary Differential Equations (with HomCont)*, Technical Report, Concordia University, 1997.
[11] J. Guckenheimer, P. Holmes, *Nonlinear Oscillations, Dynamical Systems, and Bifurcations of Vector Fields*, Springer, New York, 1990.
[12] A.H. Nayfeh, B. Balachandran, *Applied Nonlinear Dynamics, Wiley Series in Nonlinear Science*, Wiley, New York, 1995.
[13] S.H. Strogatz, *Nonlinear Dynamics and Chaos*: *with Applications to Physics, Biology, Chemistry, and Engineering*, Cambridge University Press, Perseus Publishing, 2000.
[14] T.S. Parker, L.O. Chua, *Practical Numerical Algorithms for Chaotic Systems*, Springer, New York, 1989.
[15] E. Gourdon, N.A. Alexander, C.A. Taylor, C.H. Lamarque, S. Pernot, Nonlinear energy pumping under transient forcing with strongly nonlinear coupling: theoretical and experimental results, *Journal of Sound and Vibration* 300 (3–5) (2007) 522–551.
[16] A.F. Vakakis, A.N. Kounadis, I.G. Raftoyiannis, Use of nonlinear localization for isolating structures from earthquake-induced motions, *Earthquake Engineering and Structural Dynamics* 28 (1999) 21–36.
[17] A.F. Vakakis, L.I. Manevitch, O. Gendelman, L. Bergman, Dynamics of linear discrete systems connected to local, essentially non-linear attachments, *Journal of Sound and Vibration* 264 (2003) 559–577.
[18] S.J. Zhu, Y.F. Zheng, Y.M. Fu, Analysis of non-linear dynamics of a two-degree-of-freedom vibration system with nonlinear damping and nonlinear spring, *Journal of Sound and Vibration* 271 (2004) 15–24.
[19] X. Jiang, D.M. Mcfarland, L.A. Bergman, A.F. Vakakis, Steady state passive nonlinear energy pumping in coupled oscillators: theoretical and experimental results, *Nonlinear Dynamics* 33 (2003) 87–102.
[20] Y. Ueda, Randomly transitional phenomena in the system governed by duffings equation, *Journal of Statistical Physics* 20 (1979) 181–196.
[21] L.N. Virgin, *Introduction to Experimental Nonlinear Dynamics; a Case Study in Mechanical Vibration*, Cambridge University Press, Cambridge, 2000.
[22] K. Kanai, Semi-empirical formula for the seismic characteristics of the ground, *Bulletin of the Earthquake Research Institute (Tokyo University)* 35 (1957) 308–325.

[23] H. Tajimi, A statistical method of determining the maximum response of a building structure during an earthquake. *Proceedings of the Second World Conference on Earthquake Engineering*, Tokyo, Vol. 2, 1960, pp. 781–797.
[24] S.L. Kramer, *Geotechnical Earthquake Engineering*, Prentice-Hall, Inc., Englewood Cliffs, NJ, 1996.
[25] T. Williams, C. Kelley, R. Lang, D. Kotz, J. John Campbell, G. Elber, A.Woo, Gnuplot v4.2.2; 2007, ⟨http://www.gnuplot.info/⟩.
[26] MatLab, *Language of Scientific Computing R2007a*, The Mathworks, 2007.
[27] Y. Tamura, A. Jeary, Foreword, *Journal of Wind Engineering and Industrial Aerodynamics* 59 (1996) v–viii.
[28] J.M.T. Thompson, S.R. Bishop, L.M. Leung, Fractal basins and chaotic bifurcations prior to escape from a potential well, *Physics Letters A* 121 (1987) 116–120.
[29] J.M.T. Thompson, H.B. Stewart, *Nonlinear Dynamics and Chaos*, second ed., Wiley, New York, 2002.
[30] N.A. Alexander, Evaluating basins of attraction in non-linear dynamical systems using an improved recursive boundary enhancement (RBE), *Journal of Sound and Vibration* 209 (1998) 443–472.
[31] N.A. Alexander, Evaluating the global characteristic of a nonlinear dynamical system with recursive boundary enhancement, *Advances in Engineering Software* 29 (1998) 707–716.
[32] Y. Starosvetsky, O.V. Gendelman, Dynamics of a strongly nonlinear vibration absorber coupled to a harmonically excited two-degree-of-freedom system, *Journal of Sound and Vibration* 312 (2008) 234–256.